INORGANIC CHEMISTRY
FRONTIERS

RESEARCH ARTICLE

View Article Online
View Journal | View Issue



Cite this: *Inorg. Chem. Front.*, 2023, **10**, 3025

# Ruthenium(II) polypyridyl complexes with π-expansive ligands: synthesis and cubosome encapsulation for photodynamic therapy of non-melanoma skin cancer†

Gina Elena Giacomazzo,‡[a] Michele Schlich, ‡[b] Luca Casula, ‡[b] Luciano Galantini, [c,d] Alessandra Del Giudice, [c,d] Giangaetano Pietraperzia,[a,e] Chiara Sinico,[b] Francesca Cencetti, [f] Sara Pecchioli, [f] Barbara Valtancoli,[a] Luca Conti, *[a] Sergio Murgia *[b,d] and Claudia Giorgi *[a]

In photodynamic therapy (PDT), Ru(II) polypyridyl complexes (RPCs) featuring the popular π-expansive benzo[*i*]dipyrido[3,2-*a*:2′,3′-*c*]phenazine (dppn) ligand have attracted much attention, mainly due to the good singlet oxygen sensitizing properties imparted by this peculiar ligand. However, notwithstanding the intriguing perspectives, much remains to be explored about the use of RPC-based photosensitizing agents (PSs) with more than a dppn ligand in their scaffolds. Herein, two bis-heteroleptic RPCs of the general formula $[Ru(dppn)_2L]^{n+}$ (L = 4,4′-dimethyl-2,2′-bipyridine, *n* = 2, **Ru1** or 2,2′-bipyridine-4,4′-dicarboxylate, *n* = 0, **Ru2**) were prepared in good yields by adopting an alternative synthetic approach to previously reported methods. The optimal singlet oxygen sensitizing properties and capabilities to interact with DNA displayed by **Ru1** and **Ru2** were paralleled by a potent light-triggered toxicity ($\lambda_{max}$ = 462 nm) exerted on squamous epithelial carcinoma cells. To improve the biopharmaceutical properties of these compounds, **Ru1** and **Ru2** were encapsulated into cubosomes, soft nanoparticles with a lyotropic liquid crystalline core. *In vitro* studies probed the effectiveness of these formulations against light-irradiated cancer cells and confirmed intracellular ROS generation as the mechanism likely to be responsible for the observed PDT efficacy. This work highlights the potential of $[Ru(dppn)_2L]$-based PSs in PDT, beyond providing a general and straightforward synthetic route for the preparation of this class of compounds. To the best of our knowledge, this is also the first example of the encapsulation of a RPC into cubosome nanostructures, paving the way for the development of nano-formulations with augmented biopharmaceutical properties for PDT application.

Received 16th December 2022,
Accepted 6th April 2023

DOI: 10.1039/d2qi02678c

rsc.li/frontiers-inorganic



## Introduction

Photodynamic therapy (PDT) continues to attract increasing attention thanks to the encouraging results that its application has led to the treatment of a variety of cancers, spanning from skin tumors to lung, bladder and prostate cancers,[1,2] as well as bacterial infections.[3,4] The main advantage of this therapeutic approach, which consists of the light activation of a prodrug, called a photosensitizer (PS), to produce harmful reactive oxygen species (ROS), is represented by the complete spatio-temporal control over drug activation, which provides a precious chance to limit the severe side effects normally occurring with standard chemotherapeutics.

Ruthenium(II) polypyridyl complexes (RPCs) have been largely employed in the research of suitable PSs in PDT, with the Mc Farland compound TLD1433 being the first Ru(II)-based PS to enter human clinical trials for bladder cancer.[5–8]

[a]*Department of Chemistry "Ugo Schiff", University of Florence, Via della Lastruccia 3, 50019 Sesto Fiorentino (FI), Italy. E-mail: luca.conti@unifi.it, claudia.giorgi@unifi.it*
[b]*Department of Life and Environmental Sciences, University of Cagliari, 09124 Cagliari (CA), Italy. E-mail: murgias@unica.it*
[c]*Department of Chemistry, University of Rome La Sapienza, P.le A. Moro 5, 00185 Rome, Italy*
[d]*CSGI, Consorzio Interuniversitario per lo Sviluppo dei Sistemi a Grande Interfase, 50019 Sesto Fiorentino (FI), Italy*
[e]*European Laboratory for Non-Linear Spectroscopy (LENS), Via Nello Carrara 1, 50019 Sesto Fiorentino (FI), Italy*
[f]*Department of Experimental and Clinical Biomedical Sciences "Mario Serio", 50134 Florence, Italy*

†Electronic supplementary information (ESI) available: Methods, supplementary figures and schemes, and the spectra of compounds. See DOI: https://doi.org/10.1039/d2qi02678c

‡These authors contributed equally.

The interest towards this versatile class of compounds can be attributed to its rich chemical–physical repertoire, which includes a variety of excited-state electronic configurations accessible with light, good singlet oxygen sensitizing properties, and the capacity to interact with key biological targets (such as DNA or proteins).[9–11] Of relevance is that a fine choice of ligands in their octahedral geometries permits convenient modulation of the photophysical, photochemical, and photobiological properties of the resulting RPCs, in an effort to improve cellular uptake,[12,13] shift the absorption profiles towards red,[14] confer targeting ability,[15,16] and boost $^1O_2$ sensitization. With regard to the latter aim, as prolonged excited state lifetimes are important for efficient energy transfer to molecular oxygen to form $^1O_2$, changing the nature of the lowest-lying excited state from metal-to-ligand charge-transfer ($^3$MLCT) to long-lived intraligand $^3$IL states represents a suitable way to endow the resulting RPCs with augmented cytotoxicity.[6,17] Following this strategy, over the past few years much interest has been devoted to the use of the π-expansive benzo[*i*]dipyrido[3,2-*a*:2′,3′-*c*]phenazine (dppn) ligand in the rational design of RPC-based PSs. Indeed, this peculiar ligand has been largely exploited not only to improve the photobiological activity of the resulting compounds, *via* the population of long-lived dppn-centered $^3\pi\pi^*$ excited states, but also to shift their $^1$MLCT absorption towards longer wavelengths[18] and, given its known DNA-intercalating properties, to strengthen their interaction with the nucleic acid.[19–21] A recent example of this was reported by Zhao and coworkers, who showed the benefits derived from the substitution of a bpy (bipyridine) unit by a dppn ligand in their tris-heteroleptic RPC-based PSs.[22]

Notwithstanding the advantages derived from the use of dppn, it is surprising that PSs containing two dppn ligands simultaneously coordinated to a Ru(II) center have been only sparingly explored,[23,24] while numerous examples of dppn-containing RPCs for PDT are reported in the literature[25–31] (some of them have also been applied for compounds at the boundary between PDT and photoactivated chemotherapy PACT).[32,33] Such net discrepancy between RPCs containing one and two dppn units would be related to synthetic issues concerning the preparation of the latter compounds by the general procedures for bis-heteroleptic Ru(II) complexes,[34,35] involving the intermediate [(dppn)$_2$RuCl$_2$] which is scarcely soluble in most organic solvents.

In addition, the potential anticancer activity of these systems might be limited by their common hydrophobic nature, leading to poor bioavailability and compromised therapeutic outcomes. To overcome these limits, nanocarriers have been widely investigated as a formative approach to increase the water solubility of insoluble drug candidates, prevent drug degradation, and enhance their delivery.[36–38] In the midst of the innovative exploited nano-systems, great interest has arisen around cubosomes, also known as bicontinuous cubic liquid crystalline nanoparticles with a three-dimensional arrangement of the lipid bilayer forming a honeycomb-like inner structure. Compared to single-bilayer liposomes, cubosomes are characterized by an inner portion completely filled with the lipid matrix, providing a greater hydrophobic volume and thus a higher loading efficiency.[39] Despite the fact that some investigations illustrated a possible cubosome cytotoxicity,[40,41] appropriate formulation strategies and administration at lower concentrations can be used to achieve the desired therapeutic effects. In fact, recent studies have proven their useful biomedical applications for diagnostic purposes, anticancer activity, and PDT.[42–46]

Prompted by this scenario, herein we explored the potential as PSs of two Ru(II) compounds featuring two dppn ligands simultaneously coordinated to the Ru(II) centers; [Ru(dppn)$_2$(dmbpy)]$^{2+}$ (**Ru1**) and [Ru(dppn)$_2$(dcbpy$^{2-}$)] (**Ru2**) (dmbpy = 4,4′-dimethyl-2,2′-bipyridine, dcbpy$^{2-}$ = 2,2′-bipyridine-4,4′-dicarboxylate) (Chart 1). Besides the Ru(dppn)$_2$-core, different dmbpy and dcbpy$^{2-}$ ancillary ligands were chosen to provide a potential synthetic platform for obtaining differently functionalized (dppn)$_2$-RPCs, to investigate their possible influence on the chemical–physical and biological properties of the resulting compounds.

**Ru1** and **Ru2** were prepared by adopting a straightforward synthetic route where the dppn ligands were allowed to react with Ru(II)-intermediates in the last step of the reaction, thus avoiding the use of [Ru(dppn)$_2$Cl$_2$] and leading to the production of RPCs in good yields. These systems exhibited promising features as PSs, by virtue of optimal singlet oxygen sensitizing properties and capacity to interact with DNA, and for this reason their phototoxicity and biocompatibility were tested on non-melanoma skin cancer cells *in vitro*, a model tumor selected for the feasibility of its treatment by photodynamic therapy.[47] To further ascertain their potential as PSs, **Ru1** and **Ru2** were also encapsulated in monoolein-based cubosomes stabilized with Pluronic F108. Following a preliminary investigation of the obtained formulations, **Ru2-cubo** was then selected for further development including a thorough physicochemical characterization and the assessment of its phototoxic activity against epidermoid carcinoma cells.

The results herein discussed may provide fundamental knowledge for the design of novel and highly performant PSs

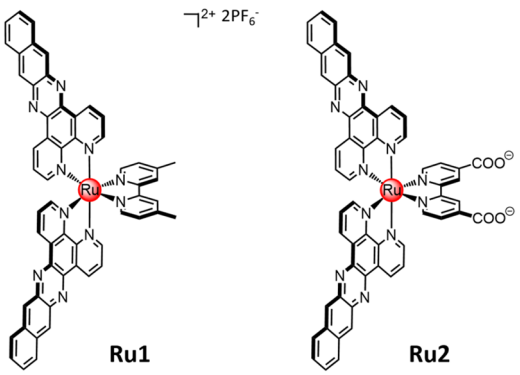


**Chart 1** Chemical structures of ruthenium complexes **Ru1** and **Ru2** of this study.

based on $(dppn)_2$-containing RPCs. Moreover, to the best of our knowledge, this study reports the first example of the encapsulation of a RPC into cubosome nanostructures, thus paving the way for the development of pharmaceutically viable nano-formulations for PDT applications.

## Results and discussion

### Synthesis and characterization of ruthenium compounds

Ru(II) complexes **Ru1** and **Ru2** were obtained *via* stepwise ligand addition following the synthetic route shown in Scheme 1c. In this synthetic approach, the polymeric precursor $[Ru(CO)_2Cl_2]_n$ was first prepared by the reaction of the commercial $RuCl_3{\cdot}nH_2O$ with paraformaldehyde in formic acid. Then, this compound was allowed to react with the bidentate ligands in refluxing methanol (dmbpy) or DMF (dcbpy), affording the *trans*-Cl[Ru(dmbpy)$(CO)_2Cl_2$] and *trans*-Cl[Ru(dcbpy)$(CO)_2Cl_2$] intermediates, with yields of 75 and 55%, respectively. In the latter case, DMF was chosen as the solvent because of the limited solubility of dcbpy in methanol.[48] Finally, two equivalents of dppn ligands were added to solutions of the *trans*-Cl[RuL$(CO)_2Cl_2$] (L = 4,4′-dimethyl-2,2′-bipyridine or dmbpy, 2,2′-bipyridine-4,4′-dicarboxylic acid or dcbpy) intermediates in 2-methoxyethanol, and in the presence of trimethylamine *N*-oxide (TMAO), to favour the detachment of the strongly coordinated CO ligands[49] and allow their replacement by the bidentate dppn ligands. The addition of aqueous $KPF_6$ led to the precipitation of the hexafluorophosphate salt of **Ru1** whereas **Ru2** precipitated as a neutral product from the reaction mixture. **Ru1** and **Ru2** were obtained, after purification by flash chromatography, in 78% and 50% yields, respectively. The identity of the obtained compounds was confirmed by $^1H$, $^{13}C$, COSY and HSQC NMR and high-resolution mass spectrometry (HR-MS) analysis (see the ESI, Fig. S1–S10†). $^1H$ NMR signal assignment is reported in the ESI;† recording of $^{13}C$ and HSQC spectra of **Ru2** was prevented by its poor solubility in $(CD_3)_2SO$.

As shown in Scheme 1, it can be highlighted that, compared to the most employed synthetic approach used for the preparation of bis-heteroleptic complexes with the general formula $[Ru(NN)_2L]^{2+}$ (*N*,*N* = polypyridyl bidentate ligand)[50,51] (Scheme 1a), commonly obtained by the reaction of $[Ru(NN)_2Cl_2]$ with a third chelate ligand (L), in the method of this work the two dppn ligands are allowed to react with the Ru(II)-scaffolds only in the last step of the reaction. This would permit to overcome solubility issues arising from the use of the $[Ru(dppn)_2Cl_2]$ intermediate. A similar "*reverse*" concept was also previously applied by Turro and coworkers in the synthesis of a rare example of a $(dppn)_2$-containing RPC reported in the literature, namely $[Ru(bpy)(dppn)_2][PF_6]_2$,[24] which was indeed obtained by the reaction of dppn with $[Ru(bpy)(CH_3CN)_4]^{2+}$ in the last reaction step (Scheme 1b). However, long reaction times (in the order of 7–24 days) were required by this route to prepare the intermediate $[Ru(bpy)(CH_3CN)_4]^{2+}$ using $RuCl_3{\cdot}nH_2O$ as the starting material.[52,53]

In light of these considerations, the synthetic strategy employed in this work may provide an alternative and straightforward way for the preparation of RPCs featuring the general formula $[Ru(dppn)_2L]^{n+}$ (L = variously functionalized bidentate polypyridyl chelates), in good yields and reaction times.

The electronic absorption spectra of **Ru1** and **Ru2** in acetonitrile are shown in Fig. 1a, whereas their molar extinction coefficients ($\varepsilon$) at different absorption maxima ($\lambda_{max}$) are listed

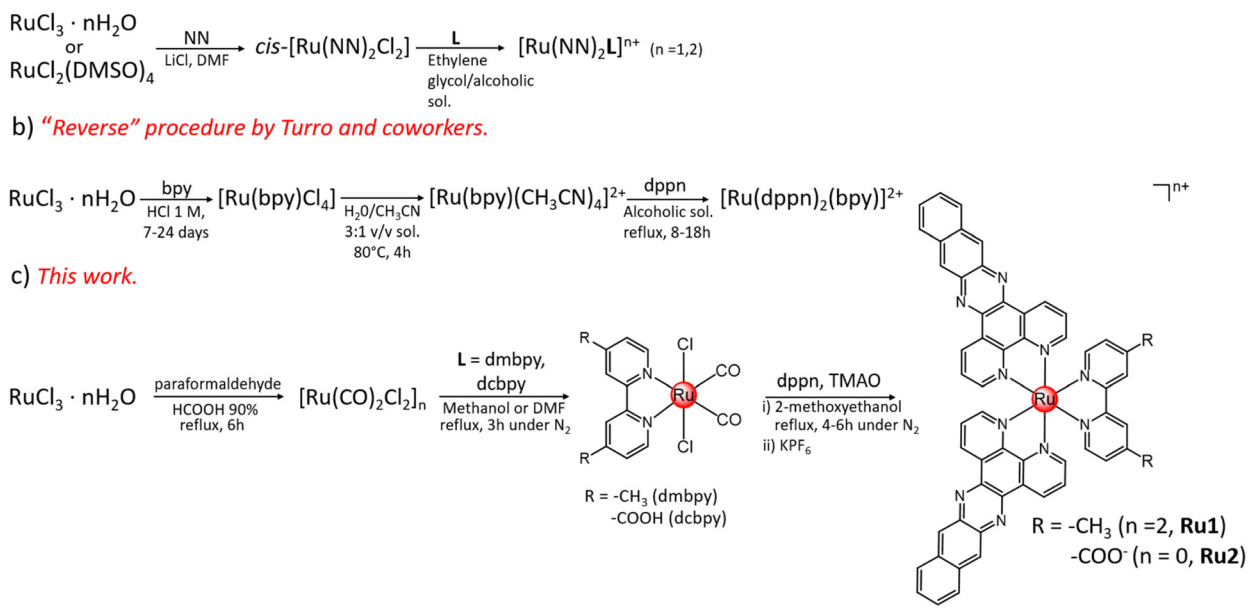


**Scheme 1** Synthetic route followed for the preparation of complexes **Ru1** and **Ru2** of this work (3c), compared to the one generally employed for the preparation of bis-heteroleptic RPCs (3a) and to the one previously reported for the Turro's compounds $[Ru(bpy)(dppn)_2][PF_6]_2$ and $[Ru(phpy)(dppn)_2][PF_6]$ (3b).

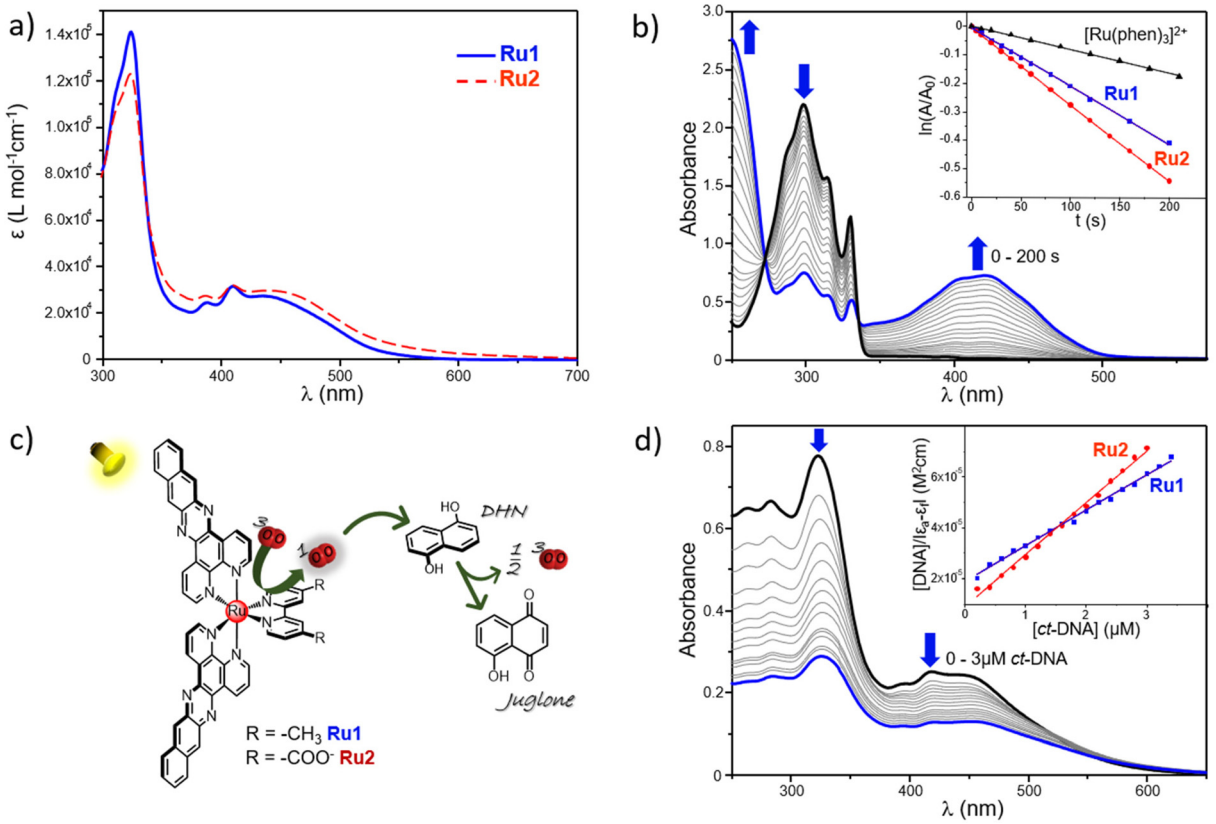


**Fig. 1** Electronic absorption spectra of **Ru1** and **Ru2** in acetonitrile (a). Singlet oxygen determination as evaluated through UV-Vis analysis by using DHN as an indirect $^1O_2$ reporter; in the inset are compared the semilogarithmic plots of $\ln(A/A_0)$ as a function of the irradiation time registered for **Ru1** and **Ru2** and $[Ru(phen)_3]^{2+}$ as the reference control ([DHN] = $3.3 \times 10^{-4}$ M, [**Ru1**] = [**Ru2**] = 10 μM) (b). Sketch of the $^1O_2$ determination by employing DHN as an indirect probe for $^1O_2$ (c). Absorption spectra of aqueous solutions of **Ru1** registered in the presence of increasing concentrations of *ct*-DNA; in the inset are reported the $[DNA]/|\varepsilon_a - \varepsilon_f|$ values obtained for **Ru1** and **Ru2** *versus* the molar concentration of DNA ([**Ru1**] = [**Ru2**] = 10 μM, TRIS buffer pH 7.4) (d).

**Table 1** Electronic absorption maxima measured in acetonitrile, rate constants $K_{obs}$, quantum yields for $^1O_2$ generation ($\phi_\Delta$) and binding constants with *ct*-DNA ($K_b$) of ruthenium complexes of this study

| Compound | $\lambda_{abs}$ nm$^{-1}$ ($\varepsilon \times 10^3$ M$^{-1}$ cm$^{-1}$)[a] | $K_{obs}$[a] | $\phi_\Delta$ ($^1O_2$)[b] | $K_b$ ($\times 10^6$ M$^{-1}$) | p$K_a$ |
|---|---|---|---|---|---|
| **Ru1** | 324 (146.1), 387 (25.3), 409 (32.2), 440 (26.6) | $1.85 \times 10^{-3}$ | 0.54 ± 0.06 | $7.49 \times 10^5$ | –– |
| **Ru2** | 323 (123.2), 387 (27.8), 410 (32.4), 445 (30.0) | $2.71 \times 10^{-3}$ | 0.50 ± 0.07 | $2.34 \times 10^6$ | p$K_{a1}$, p$K_{a2}$° 3.6 ± 0.3, p$K_{a2}^*$ 4.6 ± 0.4 |

[a] Determined in acetonitrile. [b] Determined for air-saturated acetonitrile solutions of Ru(II) complexes.

in Table 1. As shown, besides the intense intraligand π → π* transitions at 280–330 nm, both complexes display a double humped absorption at ~387 and ~410 nm, which is typical of the dppn centered π → π* transitions, plus a broad $^1$MLCT absorption centered at ~445 nm, in good agreement with those of dppn-containing RPCs reported in the literature.[24,54] It can also be noted that the absorptions relative to the dppn-centered transitions of **Ru1** and **Ru2** are more intense than the corresponding ones reported for the parental compound $[Ru(bpy)_2dppn]^{2+}$,[24] as expected due to the presence of two dppn units in their Ru(II) scaffolds. On the other hand, **Ru1** and **Ru2** resulted to be weakly luminescent, with the highest emission being displayed by **Ru2** in acetonitrile and ethanol (Fig. S11, ESI†).

Finally, given the presence of the ionizable dcbpy ligand in **Ru2**, the acid–base behavior of this complex in water was examined by means of spectrophotometric titrations, as described in the ESI.† Similar to what was previously reported for a parental dcbpy-containing Ru(II) complex,[55] of the two possible protonation equilibria only p$K_{a2}$ values of 3.6 ± 0.3 and 4.6 ± 0.4, respectively, for the ground (p$K_{a2}$°) and the excited state (p$K_{a2}^*$) (Table 1) were determined by these measurements. This, along with the presence of two inflection points in the fluorescence titrations, suggested that the first

 

$pK_a$ value was too low to be accurately determined. The higher value found for $pK_{a2}^*$ relative to $pK_{a2}°$ would be in line with the higher basicity of the complex in the excited state. It should also be noted that these data confirm that the carboxylic functions of **Ru2** are likely to be fully deprotonated at neutral pH, conferring an overall total neutral charge to the complex. Therefore, along with the different nature of their ancillary ligands, it can be envisaged that the different charges of metal complexes in physiological media (+2 for **Ru1**, 0 for **Ru2**) might have an influence on their biological behavior and interaction with cubosome nanostructures (*vide infra*).

### Singlet oxygen sensitizing properties of Ru(II)-complexes and DNA interaction

A crucial requisite for a candidate PS for PDT applications relies on its ability to trigger the formation of harmful reactive species under light-irradiation, such as the highly oxidant singlet oxygen $^1O_2$, the classical warhead of PDT produced as the result of *type*-II-based pathways.[56]

The singlet oxygen sensitizing properties of Ru(II) complexes **Ru1** and **Ru2** were first assessed spectrophotometrically, by employing 1,5-dihydroxynaphtalene (DHN) as an indirect reporter for singlet oxygen. Indeed, in the presence of $^1O_2$, DHN is promptly and quantitatively oxidized to give 5-hydroxy-1,4-naphthalenedione (Juglone), thus allowing to easily follow the photoexcitation process by monitoring the decrease of the DHN absorption band, centered at 297 nm, and the simultaneous increase of the broad Juglone band at around 427 nm (see Fig. 1c for a schematic illustration of the $^1O_2$ analysis by the DHN method for **Ru1** and **Ru2** complexes).

Fig. 1b shows the absorption spectra of an acetonitrile solution containing **Ru1** and DHN subjected to increasing irradiation times (LED emitting at 434 nm, 160 mW), light-exposure determined the progressive decrease of the DHN absorption band along with the simultaneous increase of that of Juglone, thus clearly demonstrating the photosensitizing properties of **Ru1**. It should also be noted that the appearance of two clear isosbestic points in the UV-Vis titration, at ~280 and 330 nm, ruled out the formation of long-lived intermediates or byproducts. An analogous behavior was displayed by **Ru2**, as reported in Fig. S13 of the ESI.† Compared to $[Ru(phen)_3]^{2+}$, taken as a reference RPC for $^1O_2$ sensitization, both **Ru1** and **Ru2** exhibited remarkably higher photosensitizing features. This can be easily appreciated from the corresponding semilogaritmic plots of $\ln(A/A_o)$ over the irradiation time frame ($A_0$ and $A$ are the absorbance values at 297 nm at time "*zero*" and at a generic time "*t*") reported in the inset of Fig. 1b, in which can be evidenced, for example, that a similar amount of $^1O_2$ was produced within 65–75 s by **Ru1** and **Ru2**, and in more than 200 s by $[Ru(phen)_3]^{2+}$. In detail, **Ru1** and **Ru2** displayed a comparable potency, as denoted by the slight differences emerging between their relative rate constants for the DHN photooxidation processes ($k_{obs}$), of $1.85 \times 10^{-3}$ and $2.71 \times 10^{-3}$, respectively (Table 1). In addition to the indirect DHN method, the $^1O_2$ sensitizing properties of **Ru1** and **Ru2** were further probed through direct measurement of the phosphorescence signal of $^1O_2$ at 1270 nm, induced by irradiation of air-saturated acetonitrile solutions of ruthenium complexes. This allowed us to determine the relative quantum yields of $^1O_2$ generation ($\phi_\Delta$), which are listed, along with the one of $[Ru(phen)_3]^{2+}$ for comparison ($\phi_\Delta = 0.38 \pm 0.06$), in Table 1. As shown, $\phi_\Delta$ values of $0.54 \pm 0.06$ and $0.50 \pm 0.07$ were respectively obtained for **Ru1** and **Ru2**, thus confirming that the simultaneous presence of two dppn units into the Ru(II) scaffolds confers to these complexes a potent and comparable ability to sensitize the formation of singlet oxygen, in well agreement with the results of the UV-Vis analysis.

Since it is known that $^1O_2$ rapidly reacts with the surrounding biological substrates (estimated half-life <40 ns, range of action in the order of 20 nm),[57] leading to an extremely localized oxidative damage, the ability of a PS to effectively interact with a desired biological target may be important for its potential application in PDT, as it would ensure drug localization in close proximity to the target to be treated, strengthening the oxidative damage induced by ROS sensitization. This, along with the known DNA intercalating properties imparted by the π-expansive dppn ligands, prompted us to consider the affinity of the studied RPCs with the nucleic acid. The DNA-binding abilities of **Ru1** and **Ru2** were evaluated on *calf thymus* (*ct*-DNA) through UV-Vis analysis, by monitoring the changes in the absorption profiles of the aqueous solution of RPCs buffered at pH 7.4 induced by increasing concentrations of *ct*-DNA. As shown in Fig. 1d for a 10 μM solution of **Ru1**, the addition of *ct*-DNA resulted in a strong hypochromism in both the MLCT and $\pi \rightarrow \pi^*$ absorption bands of the metal complex, with a reduction of approximately 50 and 65% of their relative intensities in the presence of only 3 μM DNA. No blue or red shift was observed upon the addition of DNA and a very similar trend was also observed in the case of **Ru2** (see Fig. S14, ESI†). The intrinsic binding constants ($K_b$) of **Ru1** and **Ru2** were calculated from titration data (see the inset of Fig. 1d for a comparison between the two RPCs) as described in the ESI† and the resulting values are reported in Table 1. As shown, $K_b$ values of $7.49 \times 10^5$ $M^{-1}$ and $2.34 \times 10^6$ $M^{-1}$ were respectively obtained for **Ru1** and **Ru2**, thus confirming the ability of these systems to strongly interact with DNA under abiotic conditions. It can be noted that these values are in line with the ones reported for other dppn-containing ruthenium complexes ($K_b$ in the order of $10^6$ $M^{-1}$)[54,58,59] and though not conclusive, together with the large extent of hypochromism observed, they hint at the intercalation as the most likely binding mode for these complexes. Moreover, the possible beneficial role played by the presence of a second dppn ligand in strengthening the interaction of complexes with the biopolymer is particularly evidenced by comparing **Ru1** with its mono-dppn containing analogue, $[Ru(dmbpy)(dppn)]^{2+}$, for which a lower $K_b$, of almost 5.8-fold has been reported.[28]

### Cytotoxicity and photoactivity of Ru(II)-complexes

To be qualified as a potential agent for photodynamic therapy, newly developed photosensitizers should be biologically inert in the dark, but highly cytotoxic when exposed to light of a

given wavelength.[60] This simple mechanism allows for selective action against the light-exposed area (*i.e.* the tumor), abolishing the systemic toxicity typically associated with traditional chemotherapeutic drugs.[46] Here, the anticancer activity of **Ru1** and **Ru2** was evaluated on A431 cells, an *in vitro* model of human epidermoid carcinoma.

As shown in Fig. 2, both compounds were found to be well tolerated by cells when no light was provided to the culture dishes. A slight difference between their *in dark* toxicities was observed, thus indicating that seemingly small modifications on the groups gathered on the bpy moieties of complexes (methyl or carboxylic functions) may influence their toxicity. In details, cell viability was reduced to 75.1 ± 4.1% and 82.4 ± 2.0% upon exposure to the highest dose of **Ru1** and **Ru2** (25 μM) in the dark, respectively. Conversely, 30-minutes of irradiation with an LED array ($\lambda_{max}$ = 462 nm, 18 mW cm$^{-2}$) induced potent activation of the complexes, triggering complete cell death (viability < 10%) at concentrations of 0.25 μM (**Ru1**, Fig. 2a) and 5 μM (**Ru2**, Fig. 2b): Fig. 2c summarizes the $IC_{50}$ values calculated from *in vitro* experiments. As shown, both **Ru1** and **Ru2** displayed high photo-toxic indexes (PI, defined as $IC_{50}$ in the dark/$IC_{50}$ upon irradiation), with values exceeding 988 and 130, respectively. From a translational point of view, higher PIs are predictive of a larger therapeutic window, with limited off-target cytotoxicity and enhanced on-target potency. Of note, notwithstanding the lack of data for the phototoxicity of dppn-containing Ru(II) complexes in A431 cells, it can be highlighted that the *in vitro* therapeutic outcomes of complexes of this study are ones of the highest among those reported in the literature for the PDT effect of dppn-containing RPCs.[23,25,61–63]

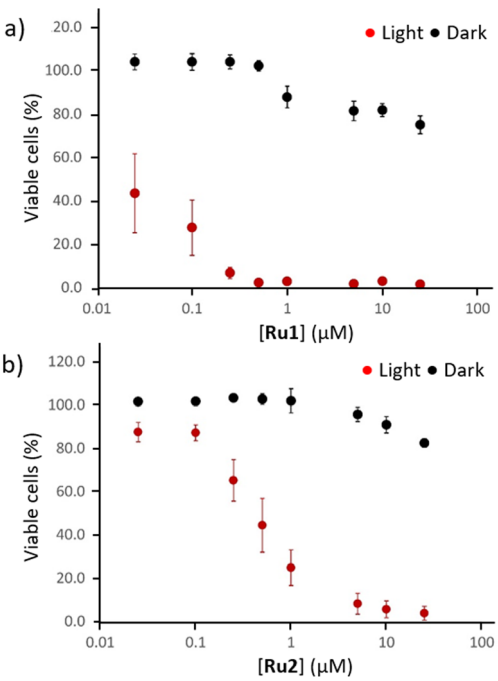


c)

| | Light | Dark |
|---|---|---|
| $IC_{50}$ **Ru1** | 0.0253 ± 0.0107 μM | > 25 μM |
| $IC_{50}$ **Ru2** | 0.191 ± 0.023 μM | > 25 μM |

**Fig. 2** Viability of A431 epidermoid carcinoma cells assessed by MTT following treatments with **Ru1** (a) or **Ru2** (b), with or without exposure to light for 30 minutes ($n$ = 5). Table summarizing the $IC_{50}$ values (±SEM) for the different experimental groups (c).

### Cubosome loading and characterization

The *in vitro* results highlighted the promising activity of the obtained systems in PDT. Nevertheless, their poor aqueous solubility would not be compatible with direct administration to a patient. In fact, self-aggregation phenomena might occur due to the high hydrophobicity of these systems, leading to low bioavailability, possible off-target activation and reduction of their photosensitivity and photophysical properties.[64] The encapsulation of PSs into nanocarriers is a well-known technique used to overcome these issues and to facilitate their biomedical application.[65] In this study, we prepared **Ru1** and **Ru2** cubosome-loaded formulations using monoolein (MO) as the molecular building block and PF108 as the stabilizing agent. In line with previous results,[66] the obtained samples were fluid aqueous dispersions with a milky macroscopic appearance. Cubosomes, here proposed as PS carriers, were prepared as described in paragraph 4.1 of the ESI† and characterized in terms of encapsulation efficiency and colloidal properties, namely size, size distribution and zeta potential.

Unencapsulated PSs were removed by exhaustive dialysis, then cubosomes were dissolved in methanol and the drug content was spectrophotometrically quantified. The results revealed high encapsulation values of **Ru2** (60%), whereas the amount of encapsulated **Ru1** was 9%. Besides their different structures, the two complexes also display different overall charges (at neutral pH **Ru1** features a double positive charge whereas **Ru2** is likely to be present in its neutral form) and this can be reasonably assumed to affect the encapsulation efficiency into cubosomes. Indeed, the production procedure and the excipients employed were identical for both formulations, the encapsulated PS being the sole difference.

As for the colloidal properties, DLS analysis revealed the presence of nanoparticles with an average diameter of approximately 138 and 142 nm, for **Ru1-cubo** and **Ru2-cubo** respectively (Fig. 3a). Both formulations showed a narrow size distribution with PDI values below 0.2. Concerning the nanoparticle zeta potential, we recorded a value of −9 mV for **Ru1-cubo** and −30 mV for **Ru2-cubo**, thus indicating a superior stabilization of the latter.

We monitored the average diameter, PDI and zeta potential over a period of 30 days, for a medium-term stability study of the colloidal systems (Fig. S16, ESI†). The size distribution study revealed optimal stability of **Ru2-cubo**, since the mean diameter did not vary appreciably during the 30 days on storage at 25 °C, with an average diameter of approximately 140 nm during the whole study. The PDI and zeta potential were almost constant, confirming the retention of the fairly narrow size distribution on storage. Conversely, the average

 

a)

| | Composition (% w/w) | | | | | Characterization | | | |
|---|---|---|---|---|---|---|---|---|---|
| | MO | PF108 | **Ru1** | **Ru2** | $H_2O$ | D (nm) | PDI | ZP (mV) | EE % |
| **Ru1-cubo** | 3.3 | 0.03 | 0.02 | - | 96.65 | 138 ± 2 | 0.11 ± 0.02 | -13 ± 3 | 9 ± 3 |
| **Ru2-cubo** | 3.3 | 0.03 | - | 0.02 | 96.65 | 142 ± 1 | 0.13 ± 0.01 | -30 ± 2 | 60 ± 5 |

b)

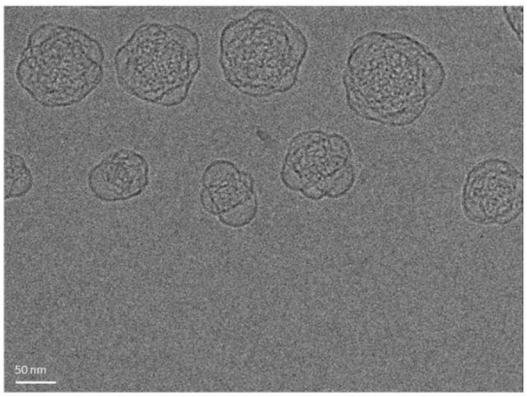


c)

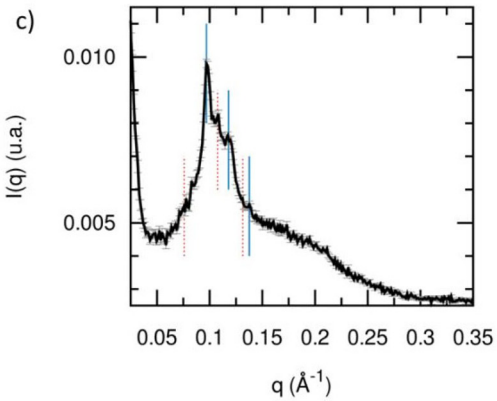


**Fig. 3** **Ru1-cubo** and **Ru2-cubo** composition and characterization in terms of average diameter (*D*, nm), polydispersion index (PDI), zeta potential (ZP, mV) and encapsulation efficiency (EE%) (a). Cryo-transmission electron microscopy (b) and small angle X-ray scattering patterns of **Ru2-cubo** with indication of the Bragg peaks corresponding to the Im3 m (red dotted lines) and the Pn3 m (blue continuous lines) cubic bicontinuous phases (c).

diameter of **Ru1-cubo** increased from 138 nm (day 0) to 235 nm (day 30), the zeta potential moved to lower values, while PDI values were almost steady.

Given the obtained preliminary results of **Ru1-cubo**, namely, low encapsulation efficiency and an increase of the average diameter over 30 days of storage, we selected **Ru2-cubo** for further characterization and *in vitro* bioactivity tests. Firstly, we evaluated the nanoparticles morphology of **Ru2-cubo** by means of cryo-transmission electron microscopy (Cryo-TEM). As shown in Fig. 3b, cubosomes appear as spherical nanoparticles with an internal structure characterized by a dark matrix and bright spots, which represent the lipid phase and the water channels respectively. We then evaluated the inner nanostructure of **Ru2-cubo** through small angle X-ray scattering. Particularly, the recorded SAXS pattern shown in Fig. 3c strongly suggests the simultaneous presence of two bicontinuous cubic phases, the Pn3 m and the Im3 m, respectively characterized by lattice parameters of 92 ± 1 Å and 117 ± 1 Å and water channel radii of 38 ± 1 Å and 37 ± 1 Å. In fact, the coexistence of the two phases is often observed when MO cubosomes are stabilized with Pluronics.[66,67]

### Cytotoxicity, photoactivity and ROS production of cubosomes-encapsulated Ru2

In addition to promoting solubility and stability, nanoencapsulation of photosensitizers in soft colloids has shown to improve the management of cancer in previous studies, as it allows targeted delivery and favors bio-membranes crossing.[68–71] When designing novel PS-loaded nanoparticles, it is critical to assess that the biological activity of the cargo is retained upon nano-encapsulation, and that no unspecific toxicity comes from the nanoparticle itself (*i.e.* empty vector). For such reasons, we tested the cytotoxicity (in the dark) and phototoxicity (upon LED illumination) of **Ru2-cubo** on the previously described epidermoid carcinoma model, comparing the results with the effect triggered by empty cubosomes (E-cubo, not loaded with PS). **Ru2-cubo** sensitized cancer cells to light even at a very low concentration of 0.025 μM ([**Ru2**]), with more than 50% reduction of cell viability at a dose of 0.25 μM (Fig. 4a). Calculated $IC_{50}$ for **Ru2-cubo** was 0.268 ± 0.079 μM. The slightly higher $IC_{50}$ of **Ru2-cubo** compared to free **Ru2** is expected for a nano-encapsulated molecule and can be partially explained by the lower intracellular localization of ruthenium, evidenced by inductively coupled plasma atomic emission spectrometry (ICP-AES), when entrapped in the soft lipid matrix (Fig. S17, ESI†). As expected, treatment with **Ru2-cubo** was efficacious only when coupled with LED irradiation, as cells incubated in the dark did not show signs of sufferance. The risk of unspecific toxicity of other components of the nanoformulation (*i.e.* monoolein and PF108) was ruled out by exposing cells to E-cubo under the same conditions (Fig. 4b).

To obtain preliminary information about the mechanism of the observed phototoxicity, we first investigated the production of intracellular ROS upon PDT using the 2′,7′-dichlorodihydro-

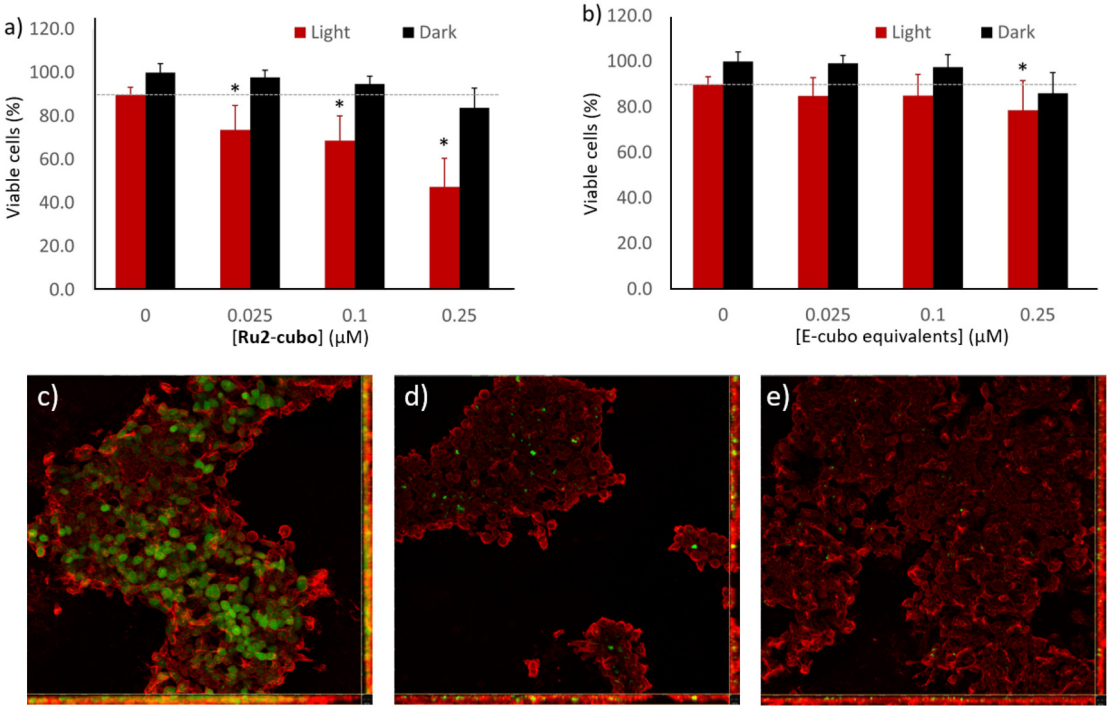


**Fig. 4** Viability of A431 epidermoid carcinoma cells assessed by MTT following treatments with **Ru2-cubo** (a) or E-cubo (b), with or without exposure to light for 30 minutes. The dose is expressed as concentration of **Ru2** in the cell culture well or the corresponding volume of E-cubo. The dashed line is a guide for the eye to highlight the viability of cells exposed to light without PS. One way ANOVA with *post-hoc* Tukey HSD test was employed to substantiate differences between cells exposed only to light (no PS, 0 μM) *vs.* cells treated with **Ru2-cubo** or E-cubo and exposed to light (*$p < 0.01$) ($n = 8$). Production of ROS by A431 epidermoid carcinoma cells estimated by the oxidation of the DCF-DA sensor and visualized by confocal laser scanning microscopy (c–e). Cells treated with **Ru2-Cubo** (100 nM) and exposed to light for 10 minutes (c) or incubated in the dark (d). Untreated cells (e). The green signal corresponds to the sensor oxidized by intracellularly produced ROS to its fluorescent derivative DCF. Red signal shows the cell membranes stained with WGA. Scalebar = 50 μm.

fluorescein diacetate (DCFH-DA) assay.[72] When applied to the cell culture, the cell permeable probe DCFH-DA crosses the cell membrane and it is deacetylated by cytosolic esterases into a non-fluorescent metabolite (DCFH). In the presence of intracellular ROS, the metabolite can be oxidized to produce highly fluorescent 2′,7′-dichlorofluorescein (DCF). The amount of ROS produced by the cells in response to PDT can be estimated by measuring the green fluorescence intensity of DCF localized within the cell body.

A431 cells were treated with **Ru2-cubo**, supplied with the DCFH-DA probe and exposed to light to trigger the activation of the photosensitizer. The dose of **Ru2-cubo** (100 nM of **Ru2**) was selected to allow for the observation of ROS generation, limiting the extent of cell toxicity. Immediately after irradiation, cells were fixed, and their membranes were stained with WGA for microscopy observation. Representative images acquired by confocal laser scanning microscopy allow to observe a diffuse green fluorescence in almost 87.4% of the cells exposed **Ru2-cubo** + light (Fig. 4c). Conversely, the treatment with **Ru2-cubo** in the dark did not induce significant production of ROS, as the amount of green signal detectable (Fig. 4d) was comparable to the one observed in a well of untreated cells (control, Fig. 4e). More specifically, the percentage of ROS-producing cells calculated through image analysis was 1.3% and 0.3% for **Ru2-cubo** in the dark and for untreated cells, respectively.

We then inspected the intracellular distribution of **Ru2-cubo** into A431 cells by employing laser-scanning confocal microscopy (Fig. S18, ESI†). Despite the ability of the PS to bind DNA, our results indicated a modest localization of **Ru2-cubo** within the nuclei, at least after 1 hour of incubation of A431 cells. This was also observed for the non-encapsulated metal complex, thus suggesting that ROS oxidation of other types of macromolecules, such as proteins or membrane lipids, rather than DNA, is likely to be the cause of the observed phototoxicity under our experimental conditions. These oxidized species, in addition to losing their function, can initiate the pro-apoptotic and pro-necrotic cascade, resulting in cell damage and death.[73]

Interestingly, it can also be noted that, in contrast to the free metal complex, which, after 1 hour of incubation, evidenced a random distribution in the cellular cytosol, after the same incubation time **Ru2-cubo** was rather found to be finely localized in discrete areas.

Overall, these results confirm that the cytotoxic effect observed upon PDT with **Ru2-cubo** would be related to the capacity of this system to effectively trigger the production of intracellular ROS, as expected due to the good singlet oxygen sensitizing properties of **Ru2**.

 

## Conclusions

In this study, we explored the potential as PSs for PDT applications of two novel Ru(II) complexes, **Ru1** and **Ru2**, characterized by two π-expansive dppn units simultaneously coordinated to their Ru(II) centers. The synthetic route followed for the preparation of these complexes may represent a valid alternative to commonly employed methods and can be potentially harnessed for the preparation of bis-heteroleptic RPCs of the general formula $[Ru(dppn)_2L]^{2+}$ (L = variously functionalized bpy ligands), whose chemical–physical and photobiological properties can be finely modulated by tuning the nature of their bidentate chelates. The simultaneous presence of two dppn ligands conferred to **Ru1** and **Ru2** optimal singlet oxygen sensitizing features and DNA-interaction capabilities, which were paralleled by a potent light-triggered toxicity exerted on squamous epithelial carcinoma cells, with PI values exceeding 988 (**Ru1**) and 130 (**Ru2**).

Given their scarce solubility in physiological media, which would preclude their direct administration for therapeutic use, **Ru1** and **Ru2** were encapsulated into cubosomes, chosen as soft nanoparticles to obtain Ru(II)-formulations with improved biopharmaceutical properties. Among the resulting hybrid systems, **Ru2-cubo** displayed superior encapsulation efficiency and stability as compared to **Ru1-cubo**, thus hinting at a subtle role played by the nature of the ancillary ligands and/or the overall charge of RPCs. For this reason, we focused our attention on the former system, which was further characterized and subjected to bioactivity investigations. Our results probed the effectiveness of **Ru2-cubo**, as denoted by the photoactivity observed even at a very low drug concentration, whereas mechanistic studies confirmed that intracellular ROS generation was likely responsible for the **Ru2-cubo**-mediated PDT efficacy.

An important aspect that deserves consideration is that soft matter nanoparticles are prone to phase transition/degradation when dispersed in fluids of biological interest.[74] However, several studies evidenced that monoolein-based cubosomes are rather stable when incubated in fetal bovine serum solution,[75,76] while when dispersed in human plasma[77] after 15 min they start to evolve towards a different kind of nanoparticle known as hexosomes, characterized by a hexagonal inner nanostructure.[78,79] Indeed, at least one investigation proved that after 10/15 min from i.v. administration in mice, cubosomes are non-altered and able to reach all the biological compartments without the release of the imaging agent they carried.

In conclusion, the results herein discussed highlight the great potential of RPCs featuring two π-expansive dppn ligands as photosensitizing agents in the blooming field of research of PDT. Going beyond providing a simple and general synthetic route for the preparation of this class of compounds, to the best of our knowledge this work also reports the first RPC to be encapsulated into cubosome nanostructures, providing fundamental knowledge about the design of pharmaceutically viable Ru(II)-cubosome formulations for PDT applications.

## Author contributions

G. E. G., M. S. and L. Casula: investigation and data curation, L. G., A. D. G., C. S., G. P., F. C., S. P. and B. V.: investigation, S. M. and C. G.: supervision and project administration, L. Conti.: writing the original draft and project administration. G. E. G., M. S., L. Casula, L. Conti, C. S., B. V., C. G. and S. M. are inventors on a pending patent application pertaining to the ruthenium polypyridyl complexes described in this work. All authors have given approval to the final version of the manuscript.

## Conflicts of interest

The authors declare no conflicts of interest.

## Acknowledgements

The authors would like to thank Dr Annalisa Guerri, from the Department of Chemistry Ugo Schiff of the University of Florence for the Cryo-TEM measurements. UniCA-Progetti biennali di Ateno Finanziati dalla Fondazione di Sardegna 2018 (CUP F741I19000950007) is gratefully acknowledged for (partial) financial support.

## References

1 G. Gunaydin, M. E. Gedik and S. Ayan, Photodynamic Therapy for the Treatment and Diagnosis of Cancer–A Review of the Current Clinical Status, *Front. Chem.*, 2021, **9**, 686303.
2 J. H. Correia, J. A. Rodrigues, S. Pimenta, T. Dong and Z. Yang, Photodynamic Therapy Review: Principles, Photosensitizers, Applications, and Future Directions, *Pharmaceutics*, 2021, **13**, 1332.
3 L. Karner, S. Drechsler, M. Metzger, A. Hacobian, B. Schädl, P. Slezak, J. Grillari and P. Dungel, Antimicrobial Photodynamic Therapy Fighting Polymicrobial Infections-a Journey from: In Vitro to in Vivo, *Photochem. Photobiol. Sci.*, 2020, **19**, 1332–1343.
4 G. Boccalini, L. Conti, C. Montis, D. Bani, A. Bencini, D. Berti, C. Giorgi, A. Mengoni and B. Valtancoli, Methylene Blue-Containing Liposomes as New Photodynamic Anti-Bacterial Agents, *J. Mater. Chem. B*, 2017, **5**, 2788–2797.
5 L. Conti, E. Macedi, C. Giorgi, B. Valtancoli and V. Fusi, Combination of Light and Ru(II) Polypyridyl Complexes: Recent Advances in the Development of New Anticancer Drugs, *Coord. Chem. Rev.*, 2022, **469**, 214656.
6 S. Monro, K. L. Colón, H. Yin, J. Roque, P. Konda, S. Gujar, R. P. Thummel, L. Lilge, C. G. Cameron and S. A. McFarland, Transition Metal Complexes and Photodynamic Therapy from a Tumor-Centered Approach: Challenges, Opportunities, and Highlights from the Development of TLD1433, *Chem. Rev.*, 2019, **119**(2), 797–828.

7 Y. Wu, S. Li, Y. Chen, W. He and Z. Guo, Recent Advances in Noble Metal Complex Based Photodynamic Therapy, *Chem. Sci.*, 2022, **13**, 5085–5106.
8 C. Mari, V. Pierroz, S. Ferrari and G. Gasser, Combination of Ru(II) Complexes and Light: New Frontiers in Cancer Therapy, *Chem. Sci.*, 2015, **6**, 2660–2686.
9 A. Notaro and G. Gasser, Monomeric and Dimeric Coordinatively Saturated and Substitutionally Inert Ru(II) Polypyridyl Complexes as Anticancer Drug Candidates., *Chem. Soc. Rev.*, 2017, **46**, 7317–7337.
10 L. Conti, G. E. Giacomazzo, B. Valtancoli, M. Perfetti, A. Privitera, C. Giorgi, P. S. Sfragano, I. Palchetti, S. Pecchioli, P. Bruni and F. Cencetti, Highly Charged Ru(II) Polypyridyl Complexes as Photosensitizer Agents in Photodynamic Therapy of Epithelial Ovarian Cancer Cells, *Int. J. Mol. Sci.*, 2022, **23**(21), 13302.
11 L. Conti, A. Mengoni, G. E. Giacomazzo, L. Mari, M. Perfetti, C. Fagorzi, L. Sorace, B. Valtancoli and C. Giorgi, Exploring the Potential of Highly Charged Ru(II)- and Heteronuclear Ru(II)/Cu(II)-Polypyridyl Complexes as Antimicrobial Agents, *J. Inorg. Biochem.*, 2021, **220**, 111467.
12 Z. Y. Yan, J. Chen, J. Shao, Z. Q. Jiao, T. S. Tang, M. Tang, Z. G. Sheng, L. Mao, R. Huang, C. H. Huang, Z. H. Zhang, H. M. Su and B. Z. Zhu, The Cell-Impermeable Ru(II) Polypyridyl Complex as a Potent Intracellular Photosensitizer under Visible Light Irradiation via Ion-Pairing with Suitable Lipophilic Counter-Anions, *Free Radicals Biol. Med.*, 2021, **171**, 69–79.
13 S. Estalayo-Adrián, S. Blasco, S. A. Bright, G. J. McManus, G. Orellana, D. C. Williams, J. M. Kelly and T. Gunnlaugsson, Water-Soluble Amphiphilic Ruthenium (II) Polypyridyl Complexes as Potential Light-Activated Therapeutic Agents, *Chem. Commun.*, 2020, **56**, 9332–9335.
14 J. Karges, F. Heinemann, F. Maschietto, M. Patra, O. Blacque, I. Ciofini, B. Spingler and G. Gasser, A Ru(II) Polypyridyl Complex Bearing Aldehyde Functions as a Versatile Synthetic Precursor for Long-Wavelength Absorbing Photodynamic Therapy Photosensitizers, *Bioorg. Med. Chem.*, 2019, **27**(12), 2666–2675.
15 L. K. McKenzie, M. Flamme, P. S. Felder, J. Karges, F. Bonhomme, A. Gandioso, C. Malosse, G. Gasser and M. Hollenstein, A Ruthenium-Oligonucleotide Bioconjugated Photosensitizing Aptamer for Cancer Cell Specific Photodynamic Therapy, *RSC Chem. Biol.*, 2022, **3**, 85–95.
16 M. Lin, S. Zou, X. Liao, Y. Chen, D. Luo, L. Ji and H. Chao, Ruthenium(II) Complexes as Bioorthogonal Two-Photon Photosensitizers for Tumour-Specific Photodynamic Therapy against Triple-Negative Breast Cancer Cells, *Chem. Commun.*, 2021, **57**, 4408–4411.
17 A. Chettri, J. A. Roque, K. R. A. Schneider, H. D. Cole, C. G. Cameron, S. A. McFarland and B. Dietzek, It Takes Three to Tango: The Length of the Oligothiophene Chain Determines the Nature of the Long-Lived Excited State and the Resulting Photocytotoxicity of a Ruthenium(II) Photodrug, *ChemPhotoChem*, 2021, **5**(5), 421–425.
18 E. C. Glazer, Panchromatic Osmium Complexes for Photodynamic Therapy: Solutions to Existing Problems and New Questions, *Photochem. Photobiol.*, 2017, **93**(5), 1326–1328.
19 A. Zamora, E. Wachter, M. Vera, D. K. Heidary, V. Rodríguez, E. Ortega, V. Fernández-Espín, C. Janiak, E. C. Glazer, G. Barone and J. Ruiz, Organoplatinum(II) Complexes Self-Assemble and Recognize AT-Rich Duplex DNA Sequences, *Inorg. Chem.*, 2021, **60**(4), 2178–2187.
20 L. E. Joyce, J. D. Aguirre, A. M. Angeles-Boza, A. Chouai, P. K. L. Fu, K. R. Dunbar and C. Turro, Photophysical Properties, DNA Photocleavage, and Photocytotoxicity of a Series of Dppn Dirhodium(II,II) Complexes, *Inorg. Chem.*, 2010, **49**(12), 5371–5376.
21 R. N. Akhimie, J. K. White and C. Turro, Dual Photoreactivity of a New Rh2(II,II) Complex for Biological Applications, *Inorg. Chim. Acta*, 2017, **454**, 149–154.
22 S. Li, J. Zhao, X. Wang, G. Xu, S. Gou and Q. Zhao, Design of a Tris-Heteroleptic Ru(II) Complex with Red-Light Excitation and Remarkably Improved Photobiological Activity, *Inorg. Chem.*, 2020, **59**(15), 11193–11204.
23 L. Wang, H. Yin, M. A. Jabed, M. Hetu, C. Wang, S. Monro, X. Zhu, S. Kilina, S. A. McFarland and W. Sun, π-Expansive Heteroleptic Ruthenium(II) Complexes as Reverse Saturable Absorbers and Photosensitizers for Photodynamic Therapy, *Inorg. Chem.*, 2017, **56**(6), 3245–3259.
24 B. Peña, N. A. Leed, K. R. Dunbar and C. Turro, Excited State Dynamics of Two New Ru(II) Cyclometallated Dyes: Relation to Cells for Solar Energy Conversion and Comparison to Conventional Systems, *J. Phys. Chem. C*, 2012, **116**(42), 17095–17101.
25 B. A. Albani, B. Peña, N. A. Leed, N. A. B. G. De Paula, C. Pavani, M. S. Baptista, K. R. Dunbar and C. Turro, Marked Improvement in Photoinduced Cell Death by a New Tris-Heteroleptic Complex with Dual Action: Singlet Oxygen Sensitization and Ligand Dissociation, *J. Am. Chem. Soc.*, 2014, **136**(49), 17095–17101.
26 C. Reichardt, S. Monro, F. H. Sobotta, K. L. Colón, T. Sainuddin, M. Stephenson, E. Sampson, J. Roque, H. Yin, J. C. Brendel, C. G. Cameron, S. A. McFarland and B. Dietzek, Predictive Strength of Photophysical Measurements for in Vitro Photobiological Activity in a Series of Ru(II) Polypyridyl Complexes Derived from π-Extended Ligands, *Inorg. Chem.*, 2019, **58**(5), 3156–3166.
27 F. Haddache, A. Le Goff, B. Reuillard, K. Gorgy, C. Gondran, N. Spinelli, E. Defrancq and S. Cosnier, Label-Free Photoelectrochemical Detection of Double-Stranded HIV DNA by Means of a Metallointercalator-Functionalized Electrogenerated Polymer, *Chem. – Eur. J.*, 2014, **20**(47), 15555–15560.
28 S. Vidhisha, K. L. Reddy, Y. P. Kumar, M. Srijana and S. Satyanarayana, Synthesis, Characterization, Antibacterial Activity and Investigation of DNA Binding for Ru(II) Molecular "Light Switch" Complexes, *Int. J. Pharm. Sci. Rev. Res.*, 2014, **25**(1), 197–205.

 

29 H. Yin, M. Stephenson, J. Gibson, E. Sampson, G. Shi, T. Sainuddin, S. Monro and S. A. McFarland, In Vitro Multiwavelength PDT with 3IL States: Teaching Old Molecules New Tricks, *Inorg. Chem.*, 2014, **53**(9), 4548–4559.

30 Q. X. Zhou, W. H. Lei, J. R. Chen, C. Li, Y. J. Hou, X. S. Wang and B. W. Zhang, A New Heteroleptic Ruthenium(II) Polypyridyl Complex with Long-Wavelength Absorption and High Singlet-Oxygen Quantum Yield., *Chem. – Eur. J.*, 2010, **16**(10), 3157–3165.

31 C. W. Jiang, H. Chao, R. H. Li, H. Li and L. N. Ji, Syntheses, Characterization and Third-Order Nonlinear Optical Properties of Ruthenium(II) Complexes Containing 2-Phenylimidazo-[4,5-f][1,10]Phenanthroline and Extended Diimine Ligands, *Polyhedron*, 2001, **20**(17), 2187–2193.

32 L. N. Lameijer, T. G. Brevé, V. H. S. van Rixel, S. H. C. Askes, M. A. Siegler and S. Bonnet, Effects of the Bidentate Ligand on the Photophysical Properties, Cellular Uptake, and (Photo)Cytotoxicity of Glycoconjugates Based on the [Ru(Tpy)(NN)(L)]2 + Scaffold, *Chem. – Eur. J.*, 2018, **24**(11), 2709–2717.

33 N. Toupin, S. J. Steinke, S. Nadella, A. Li, T. N. Rohrabaugh, E. R. Samuels, C. Turro, I. F. Sevrioukova and J. J. Kodanko, Photosensitive Ru(II) Complexes as Inhibitors of the Major Human Drug Metabolizing Enzyme CYP3A4, *J. Am. Chem. Soc.*, 2021, **143**(24), 9191–9205.

34 A. C. Munteanu, A. Notaro, M. Jakubaszek, J. Cowell, M. Tharaud, B. Goud, V. Uivarosi and G. Gasser, Synthesis, Characterization, Cytotoxic Activity, and Metabolic Studies of Ruthenium(II) Polypyridyl Complexes Containing Flavonoid Ligands, *Inorg. Chem.*, 2020, **59**(7), 4424–4434.

35 G. E. Shillito, S. E. Bodman, J. I. Mapley, C. M. Fitchett and K. C. Gordon, Accessing a Long-Lived 3LC State in a Ruthenium(II) Phenanthroline Complex with Appended Aromatic Groups, *Inorg. Chem.*, 2020, **59**(23), 16967–16975.

36 K. Sztandera, M. Gorzkiewicz and B. Klajnert-Maculewicz, Nanocarriers in Photodynamic Therapy—in Vitro and in Vivo Studies, *Wiley Interdiscip. Rev.: Nanomed. Nanobiotechnol.*, 2020, **12**(3), 1509.

37 A. Q. Annu, B. Nabi, S. Kotta, J. K. Narang, S. Baboota and J. Ali, Role of Nanocarriers in Photodynamic Therapy, *Photodiagn. Photodyn. Ther.*, 2020, **30**, 101782.

38 F. Lai, M. Schlich, R. Pireddu, F. Corrias, A. Fadda and C. Sinico, Production of Nanosuspensions as a Tool to Improve Drug Bioavailability: Focus on Topical Delivery, *Curr. Pharm. Des.*, 2015, **21**(42), 6089–6103.

39 S. Murgia, S. Biffi and R. Mezzenga, Recent Advances of Non-Lamellar Lyotropic Liquid Crystalline Nanoparticles in Nanomedicine, *Curr. Opin. Colloid Interface Sci.*, 2020, **48**, 28–39.

40 J. Barauskas, C. Cervin, M. Jankunec, M. Špandyreva, K. Ribokaite, F. Tiberg and M. Johnsson, Interactions of Lipid-Based Liquid Crystalline Nanoparticles with Model and Cell Membranes, *Int. J. Pharm.*, 2010, **391**(1–2), 248–291.

41 J. C. Bode, J. Kuntsche, S. S. Funari and H. Bunjes, Interaction of Dispersed Cubic Phases with Blood Components, *Int. J. Pharm.*, 2013, **448**(1), 87–95.

42 S. Murgia, S. Bonacchi, A. M. Falchi, S. Lampis, V. Lippolis, V. Meli, M. Monduzzi, L. Prodi, J. Schmidt, Y. Talmon and C. Caltagirone, Drug-Loaded Fluorescent Cubosomes: Versatile Nanoparticles for Potential Theranostic Applications, *Langmuir*, 2013, **29**(22), 6673–6679.

43 F. D. Victorelli, L. Salvati Manni, S. Biffi, B. Bortot, H. H. Buzzá, V. Lutz-Bueno, S. Handschin, G. Calixto, S. Murgia, M. Chorilli and R. Mezzenga, Potential of Curcumin-Loaded Cubosomes for Topical Treatment of Cervical Cancer, *J. Colloid Interface Sci.*, 2022, **620**, 419–430.

44 S. Jenni, G. Picci, M. Fornasier, M. Mamusa, J. Schmidt, Y. Talmon, A. Sour, V. Heitz, S. Murgia and S. C. Caltagirone, Multifunctional Cubic Liquid Crystalline Nanoparticles for Chemo- A Nd Photodynamic Synergistic Cancer Therapy, *Photochem. Photobiol. Sci.*, 2020, **19**, 674–680.

45 U. Bazylińska, D. Wawrzyńczyk, J. Kulbacka, G. Picci, L. S. Manni, S. Handschin, M. Fornasier, C. Caltagirone, R. Mezzenga and S. Murgia, Hybrid Theranostic Cubosomes for Efficient NIR-Induced Photodynamic Therapy, *ACS Nano*, 2022, **16**(4), 5427–5438.

46 U. Bazylińska, J. Kulbacka, J. Schmidt, Y. Talmon and S. Murgia, Polymer-Free Cubosomes for Simultaneous Bioimaging and Photodynamic Action of Photosensitizers in Melanoma Skin Cancer Cells, *J. Colloid Interface Sci.*, 2018, **522**, 163–173.

47 M. C. F. Simões, J. J. S. Sousa and A. A. C. C. Pais, Skin Cancer and New Treatment Perspectives: A Review, *Cancer Lett.*, 2015, **357**(1), 8–42.

48 M. Kubeil, R. R. Vernooij, C. Kubeil, B. R. Wood, B. Graham, H. Stephan and L. Spiccia, Studies of Carbon Monoxide Release from Ruthenium(II) Bipyridine Carbonyl Complexes upon UV-Light Exposure, *Inorg. Chem.*, 2017, **56**(10), 5941–5952.

49 N. Nickita, M. J. Belousoff, A. I. Bhatt, A. M. Bond, G. B. Deacon, G. Gasser and L. Spiccia, Synthesis, Structure, Spectroscopic Properties, and Electrochemical Oxidation of Ruthenium(II) Complexes Incorporating Monocarboxylate Bipyridine Ligands, *Inorg. Chem.*, 2007, **46**(21), 8638–8651.

50 A. Notaro, M. Jakubaszek, S. Koch, R. Rubbiani, O. Dömötör, E. A. Enyedy, M. Dotou, F. Bedioui, M. Tharaud, B. Goud, S. Ferrari, E. Alessio and G. Gasser, A Maltol-Containing Ruthenium Polypyridyl Complex as a Potential Anticancer Agent, *Chem. – Eur. J.*, 2020, **26**(20), 4997–5009.

51 E. Wachter, D. K. Heidary, B. S. Howerton, S. Parkin and E. C. Glazer, Light-Activated Ruthenium Complexes Photobind DNA and Are Cytotoxic in the Photodynamic Therapy Window, *Chem. Commun.*, 2012, **48**, 9649–9651.

52 R. A. Krause, Synthesis of Mixed Complexes of Ruthenium (II) with 2,2′-Dipyridyl, *Inorg. Chim. Acta*, 1977, **22**, 209–213.

53 A. Petroni and L. D. Slep, Etchenique, R. Ruthenium(II) 2,2′-Bipyridyl Tetrakis Acetonitrile Undergoes Selective Axial Photocleavage., *Inorg. Chem.*, 2008, **47**(3), 951–956.

54 H. K. Saeed, P. J. Jarman, S. Archer, S. Sreedharan, I. Q. Saeed, L. K. Mckenzie, J. A. Weinstein, N. J. Buurma, C. G. W. Smythe and J. A. Thomas, Homo– and Heteroleptic Phototoxic Dinuclear Metallo–Intercalators Based on Ru II (Dppn) Intercalating Moieties: Synthesis, Optical, and Biological Studies, *Angew. Chem., Int. Ed.*, 2017, **56**(41), 12628–12633.

55 T. Shimidzu, T. Iyoda and K. Izaki, Photoelectrochemical Properties of Bis(2,2′-Bipyridine)(4,4′-Dicarboxy-2,2′-Bipyridine) Ruthenium(II) Chloride, *J. Phys. Chem.*, 1985, **89**(4), 642–645.

56 C. Imberti, P. Zhang, H. Huang and P. J. Sadler, New Designs for Phototherapeutic Transition Metal Complexes, *Angew. Chem., Int. Ed.*, 2020, **59**(1), 61–73.

57 A. P. Castano, T. N. Demidova and M. R. Hamblin, Mechanisms in Photodynamic Therapy: Part One - Photosensitizers, Photochemistry and Cellular Localization, *Photodiagn. Photodyn. Ther.*, 2004, **1**(4), 279–293.

58 Y. Sun, L. E. Joyce, N. M. Dickson and C. Turro, Efficient DNA Photocleavage by [Ru(Bpy)2(Dppn)]2+ with Visible Light, *Chem. Commun.*, 2010, **46**, 2426–2428.

59 S. P. Foxon, C. Metcalfe, H. Adams, M. Webb and J. A. Thomas, Electrochemical and Photophysical Properties of DNA Metallo-Intercalators Containing the Ruthenium(II) Tris(1-Pyrazolyl)Methane Unit., *Inorg. Chem.*, 2007, **46**(2), 409–416.

60 D. Van Straten, V. Mashayekhi, H. S. de Bruijn, S. Oliveira and D. J. Robinson, Oncologic Photodynamic Therapy: Basic Principles, Current Clinical Status and Future Directions, *Cancers*, 2017, **9**(2), 1–54.

61 L. M. Lifshits, J. A. Roque, P. Konda, S. Monro, H. D. Cole, D. V. Dohlen, S. Kim, G. Deep, R. P. Thummel, C. G. Cameron, S. Gujar and S. A. McFarland, Near-infrared absorbing Ru(II) complexes act as immunoprotective photodynamic therapy (PDT) agents against aggressive melanoma, *Chem. Sci.*, 2020, **11**, 11740.

62 L. N. Lameijer, S. L. Hopkins, T. G. Brevé, S. H. C. Askes and S. Bonnet, D-Versus L-Glucose Conjugation: Mitochondrial Targeting of a Light-Activated Dual-Mode-of Action Ruthenium-Based Anticancer Prodrug, *Chem. – Eur. J.*, 2016, **22**, 18484–18491.

63 S. Li, J. Zhao, X. Wang, G. Xu, S. Gou and Q. Zhao, Design of a Tris-Heteroleptic Ru(II) Complex with Red-Light Excitation and Remarkably Improved Photobiological Activity, *Inorg. Chem.*, 2020, **59**, 11193–11204.

64 S. Moghassemi, A. Dadashzadeh, R. B. Azevedo, O. Feron and C. A. Amorim, Photodynamic cancer therapy using liposomes as an advanced vesicular photosensitizer delivery system, *J. Controlled Release*, 2021, **339**(10), 75–90.

65 C. F. de Freitas, D. S. Pellosi and A. L. Tessaro, 8-Lipid-based nanoparticles in photodynamic therapy, *in Nanomaterials for Photodynamic Therapy*, 2023, 203–226.

66 M. Fornasier, S. Biffi, B. Bortot, P. Macor, A. Manhart, F. R. Wurm and S. Murgia, Cubosomes Stabilized by a Polyphosphoester-Analog of Pluronic F127 with Reduced Cytotoxicity, *J. Colloid Interface Sci.*, 2020, **580**, 286–297.

67 A. M. Falchi, A. Rosa, A. Atzeri, A. Incani, S. Lampis, V. Meli, C. Caltagirone and S. Murgia, Effects of Monoolein-Based Cubosome Formulations on Lipid Droplets and Mitochondria of HeLa Cells, *Toxicol. Res.*, 2015, **4**, 1025–1036.

68 J. Guo, M. Schlich, J. F. Cryan and C. M. O'Driscoll, Targeted Drug Delivery via Folate Receptors for the Treatment of Brain Cancer: Can the Promise Deliver?, *J. Pharm. Sci.*, 2017, **106**(12), 3413–3420.

69 Z. Zhen, W. Tang, C. Guo, H. Chen, X. Lin, G. Liu, B. Fei, X. Chen, B. Xu and J. Xie, Ferritin Nanocages to Encapsulate and Deliver Photosensitizers for Efficient Photodynamic Therapy against Cancer, *ACS Nano*, 2013, **7**(8), 6988–6996.

70 S. Demartis, G. Rassu, S. Murgia, L. Casula, P. Giunchedi and E. Gavini, Improving Dermal Delivery of Rose Bengal by Deformable Lipid Nanovesicles for Topical Treatment of Melanoma, *Mol. Pharm.*, 2021, **18**(11), 4046–4057.

71 L. Conti, S. Ciambellotti, G. E. Giacomazzo, V. Ghini, L. Cosottini, E. Puliti, M. Severi, E. Fratini, F. Cencetti, P. Bruni, B. Valtancoli, C. Giorgi and P. Turano, Ferritin Nanocomposites for the Selective Delivery of Photosensitizing Ruthenium-Polypyridyl Compounds to Cancer Cells, *Inorg. Chem. Front.*, 2022, **9**, 1070–1081.

72 S. Wang, A. Riedinger, H. Li, C. Fu, H. Liu, L. Li, T. Liu, L. Tan, M. J. Barthel, G. Pugliese, F. De Donato, M. Scotto D'Abbusco, X. Meng, L. Manna, H. Meng and T. Pellegrino, Plasmonic Copper Sulfide Nanocrystals Exhibiting Near-Infrared Photothermal and Photodynamic Therapeutic Effects, *ACS Nano*, 2015, **9**(2), 1788–1800.

73 M. Redza-Dutordoir and D. A. Averill-Bates, Activation of Apoptosis Signalling Pathways by Reactive Oxygen Species, *Biochim. Biophys. Acta*, 2016, **1863**(12), 2977–2992.

74 A. Yaghmur and H. Mu, Recent advances in drug delivery applications of cubosomes, hexosomes, and solid lipid nanoparticles, *Acta Pharm. Sin. B*, 2021, **11**(4), 871–885.

75 S. Deshpande, E. Venugopal, S. Ramagiri, J. R. Bellare, G. Kumaraswamy and N. Singh, *ACS Appl. Mater. Interfaces*, 2014, **6**(19), 17126–17133.

76 A. Gupta, T. Stait-Gardner, L. de Campo, L. J. Waddington, N. Kirby, W. S. Price and M. J. Moghaddam, *J. Mater. Chem. B*, 2014, **2**, 1225–1233.

77 J. C. Bode, J. Kuntsche, S. S. Funari and H. Bunjes, *Int. J. Pharm.*, 2013, **448**(1), 87–95.

78 C. Caltagirone, M. Arca, A. M. Falchi, V. Lippolis, V. Meli, M. Monduzzi, T. Nylander, A. Rosa, J. Schmidt, Y. Talmond and S. Murgia, *RSC Adv.*, 2015, **5**, 23443–23449.

79 V. Meli, C. Caltagirone, C. Sinico, F. Lai, A. M. Falchi, M. Monduzzi, M. Obiols-Rabasa, G. Picci, A. Rosa, J. Schmidt, Y. Talmone and S. Murgia, *New J. Chem.*, 2017, **41**, 1558–1565.

 